Theoretical Study of Structure, Vibrational Frequencies, and Electronic Spectra of Dibenzofuran and Its Polychlorinated Derivatives

Ivan Ljubić* and Aleksandar Sabljić

Department of Physical Chemistry, Ruđer Bošković Institute, P. O. Box 180, HR-10002, Zagreb, Republic of Croatia

Received: November 16, 2006; In Final Form: December 18, 2006

Minimum structures and harmonic vibrational frequencies of dibenzofuran (DF), 2,3,7,8-tetrachlorodibenzofuran (TCDF), and octachlorodibenzofuran (OCDF) were calculated using the multiconfigurational complete active space self-consistent field (CASSCF) and density functional theory (DFT) methods. The electronic transitions in these compounds were studied via the single-state multireference second-order perturbation theory (CASPT2) based on the CASSCF(14,13) references, as well as the time-dependent DFT (TD-B3P86) employing the cc-pVDZ (CASSCF/CASPT2) and 6-31G(d,p) (TD-B3P86) basis sets. The B3P86 geometry and harmonic vibrational frequencies of ground state DF agree very well with the experimental data, and the CASSCF/CASPT2 excitation energies and oscillator strengths are accurate enough to provide a reliable assignment of the absorption bands in the 200−300 nm region. The close agreements with experiment for the parent DF give the present theoretical approaches a valuable credit in predicting the properties of the environmentally toxic polychlorinated congeners, which is all the more important considering the difficulties and hazards in obtaining the experimental data.

Introduction

The ubiquity and notorious persistence of polychlorinated dioxins (PCDDs), dibenzofurans (PCDFs), and biphenyls (PBCs) have raised particular concern since the early 1970s when the first studies on their accumulation in human tissues, food, and environment took place.[1,2] It has since been recognized that virtually every incineration of organic matter in the presence of minute amounts of inorganic and/or organic chlorine containing compounds can act as a potential source of these pollutants.[3] Thus, e.g., they were identified in tobacco smoke,[4] while on a larger scale many mundane industrial processes are involved, such as burning of coal, diesel fuel, and treated wood, or smelting of metal ores.[3] Emissions from industrial and municipal waste incinerators, as well as from backyard trash burning, received attention as a principal source in urban areas.[5]

Numerous studies have shown that many compounds in this class exhibit extreme acute toxicity and are capable of inflicting serious long-term effects as potent tumor promoters and teratogens.[6,7] The most hazardous of them, 2,3,7,8-tetrachlorodibenzo-*p*-dioxin (2,3,7,8-TCDD), serves as a standard in defining the (mammalian) toxic equivalency factor (TEF), actually an estimate of the order of magnitude of toxicity with respect to 2,3,7,8-TCDD, whose TEF is taken to be equal to 1.0.[2] For the present work we chose to study a subclass of dibenzofuran structures (Figure 1), which includes the parent dibenzofuran (DF) as a model compound, 2,3,7,8-tetrachlorodibenzofuran (TCDF), and octachlorodibenzofuran (OCDF). The TEFs of TCDF and OCDF equal 0.1 and 0.001, respectively,[2] meaning that in particular TCDF is still highly toxic.

Many experimental studies on this class of pollutants were aimed at their separation and quantitative identification in complex environmental mixtures, as well as possibilities of their

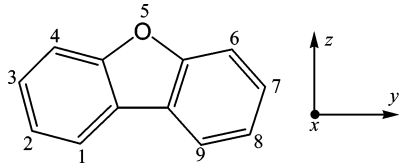

Figure 1. Enumeration of atoms and orientation of the molecule fixed coordinate system (according to IUPAC conventions[8]) in dibenzofurans.

deactivation, e.g., by UV irradiation.[9,10] Clearly, reliably determined features of the IR and UV spectra would play an indispensable role here. The majority of spectroscopic data pertains to the parent DF, often in combination with structurally similar pollutants such as fluorene and carbazole.[11−23] The IR[13,18,19] and UV[11,14,15] absorption spectra, as well as emission (fluorescence[9,16] and phosphorescence[9,17,21]) spectra, were analyzed. Combined experimental and theoretical studies[12,17,20] led to a nearly complete assignment of the bands in the IR and Raman vibrational spectra. With regard to the electronic transitions, a few earlier experimental studies in the crystal, solution, and vapor phases were assisted by semiempirical CIS calculations to rationalize the observed excitation energies and oscillator strengths.[11,12,14,15] The polarized crystal spectra enabled reliable symmetry assignments of the band systems in the 200−300 nm region.[14] Recently the ro−vibrational structure of the $S_1 \leftarrow S_0$ band was studied by employing ultrahigh-precision sub-Doppler laser excitation spectroscopy, whereby accurate rotational constants and several vibrational frequencies of the first excited state S_1 were determined.[22,23]

On the other hand, experimental studies of the toxic polychlorinated derivatives are relatively scarce, which is mostly due to the extreme precautionary measures required for their safe handling. Funk and co-workers[10] analyzed the UV absorption and laser induced fluorescence spectra of polychlorinated dibenzodioxins, dibenzofurans, and polycyclic aromatic hydrocarbons, among which are TCDF and OCDF. Their interpreta-

* Author to whom correspondence should be addressed. E-mail: iljubic@irb.hr.

10.1021/jp0676336 CCC: $37.00
Published on Web 01/25/2007

tion of spectra rests upon tentative assumptions on the origins of electronic transitions and luminescence yields, which require corroboration via reliable quantum chemical models. To our knowledge, this has not been done thus far in the case of PCDFs.

For the present study of the structure and spectroscopic properties of DF, TCDF, and OCDF, high-quality methods were chosen, viz., the complete active space self-consistent field (CASSCF) method[24] combined with the multireference second-order perturbation theory (CASPT2),[25] as well as the density functional theory (DFT) and its time-dependent variant (TD-DFT)[26] for studying the electronic spectra. Whereas DFT is expected to predict the ground state properties more accurately than CASSCF, the combined CASSCF/CASPT2 approach proved clearly superior to TD-DFT in computing the electronic transitions in polychlorinated dioxins.[27,28] Throughout the past decade CASSCF/CASPT2 has evolved as a powerful quantitative tool for rationalizing electronic spectra of a large variety of molecules.[29] TD-DFT is here intended primarily as an economical complement, in that it indicates all the electronic transitions regardless of their symmetry types. It is, however, expected to be reasonably accurate only for the lower excited states.[28]

Computational Methods

Stationary geometries and harmonic vibrational wavenumbers of the three dibenzofurans were calculated via the CASSCF method.[24] We also used DFT based upon the Becke styled three-parameter hybrid functional B3P86, which incorporates weighted portions of the Slater and Hartree−Fock (HF) exchange, Becke 1988 gradient correction, Vosko−Wilk−Nusair (local spin density) correlation, and the Perdew 1986 nonlocal correlation.[30] An advantage was given to B3P86 over the more common B3LYP, because in a previous work time-dependent B3P86 (TD-B3P86) resulted in slightly better excitation energies for a set of small organic compounds.[31] In the present work it was observed that, whereas the minimum geometries and harmonic frequencies of the three DFs differ to a certain extent between the two functionals, B3P86 does not perform inferior to B3LYP in either respect.

In CASSCF calculations we used active spaces of 14 electrons distributed among 13 active orbitals, viz., (14,13), which is completely analogous to the (16,14) active space used in our investigations on polychlorinated dioxins.[27,28] The dynamic electron correlation was accounted for via the single-state[25] and multistate[32] CASPT2 calculations with the optimized CASSCF-(14,13) wave functions as the zero-order references. It was observed, however, that multistate CASPT2 excitation energies generally coincide poorly with the single-state ones and deviate more from the available experimental data. Because the reason might be in a larger number of roots required for reliable multistate calculations, the single-state CASPT2 results are hereby trusted more. Thus, the vertical and adiabatic CASSCF/CASPT2 excitation energies were calculated as differences in the single-state CASPT2 energies between the ground and excited states.

Several other active spaces were tested. It was observed, for instance, that nothing is gained by (14,14), whereby also the oxygen lone pair would be correlated. On the contrary, in the subsequent CASPT2 calculations this active space created very serious intruder problems, as did the smallest possible (12,12) active space. Overall, for a reliable description of the valence excited states, it was essential that the active space comprises the π orbitals on the 12 carbon atoms and the out-of-plane lone pair on the oxygen atom, whereas the out-of-plane chlorine lone pairs are superfluous for that matter, and some care had to be taken to omit them from the active space. Some Rydberg transitions, typically involving diffuse states of the $3p_x$, $3d_{xz}$, and $3d_{xy}$ type, may appear around 6 eV mixing with the valence $\pi-\pi^*$ states. More detailed studies into the extent of the valence−Rydberg mixings would involve extensions of basis sets with diffuse functions, as well as expanding the present active space,[29] neither of which is currently feasible. Thus the CASSCF/CASPT2 excitation energies above the 6 eV threshold might contain some additional uncertainties. The (14,13) and (12,12) active spaces were used previously in calculations on DF and its radical cation,[33,34] albeit with a smaller basis set in the case of the (14,13). Graphic representations (using MOLDEN[35]) of the active space, as well as the relevant Kohn−Sham orbitals of the ground state DF, are included in the Supporting Information.

The CASSCF geometry optimizations were carried out by constraining the three DFs to the C_{2v} point group symmetry, which was vindicated via the subsequent harmonic wavenumber analysis. Employing the molecule fixed coordinate frame (Figure 1), the active space encompassed seven molecular orbitals (MOs) of b_1 symmetry and six of a_2 symmetry. The orbitally allowed $\pi-\pi^*$ transitions belong to the A_1 and B_2 irreducible representations, and so the state-averaged (SA) CAS calculations[36] were carried out over the six lowest equally weighted roots constraining the wave functions to the A_1 and B_2 symmetries. In addition, two SA geometric optimizations were conducted within the space of the two lowest roots to enable an estimate of the 2^1A_1 and 2^1B_2 adiabatic excitation energies. Participation of the in-plane orbitals gives rise to some low-lying, albeit expectedly weak (x-polarized) B_1, as well as orbitally forbidden A_2-type transitions. These transitions could not be described within the present π active space multiconfigurational treatment, but were contributed by the TD-B3P86 approach.

For the CASSCF/CASPT2 calculations the largest affordable basis set was the standard Dunning's correlation consistent cc-pVDZ, contracted to 4s3p1d on Cl, 3s2p1d on C and O, and 2s1p on H.[37] This amounted to 222, 274, and 326 basis functions in DF, TCDF, and OCDF, respectively. Because of the lack of basis functions to correlate properly the inner shells of the O, C, and Cl atoms, these orbitals were kept frozen in the CASPT2 calculations. Although basis sets of double-ζ quality are considered merely as minimal sensible for correlated calculations,[38] larger or more flexible basis sets currently prove prohibitive in the CASSCF/CASPT2 calculations on this scale. Notwithstanding this, by employing the cc-pVDZ basis set we managed to obtain excellent results for the electronic transitions in polychlorinated dioxins.[27,28] For the B3P86 and TD-B3P86 calculations we used the standard 6-31G(d,p) basis set,[39] which numbered 235, 291, and 347 basis functions. For the parent DF we probed the effects of diffuse and augmented sets of polarization functions on the TD-B3P86 excitation energies with the two considerably larger basis sets, cc-pVTZ and 6-311+G-(2df,2p). The benefits were largely unconvincing, however, and the large increase in computational time for the two chlorinated congeners would certainly not have been justified.

The use of the level shift (CASPT2-LS[29]) proved necessary in obtaining reliable second-order energies, particularly for the two polychlorinated derivatives. In the case of PCDFs the occurrence of intruder states (singularities) due to near zero energy denominators could always be traced to the configurations that involved excitations from the out-of-plane chlorine lone pairs absent from the active space. We used the imaginary

level shift (ILS) technique introduced by Forsberg and Malmqvist,[40] which proved efficient in the calculations on the polychlorinated dioxins.[27,28] Tests showed that the reference weights in the excited states approach to within 5% of the ground state reference weights (around 0.65, 0.57, and 0.51 for DF, TCDF, and OCDF, respectively) employing the value of ILS parameter of 0.10 hartree. Because the excitation energies were largely insensitive to increase in ILS up to 0.20 hartree, the lowest sensible value of ILS of 0.10 hartree was retained throughout. It was found to fully solve the intruder problems in all the affected states.

Combined with the CASPT2-ILS approach, the IPEA level shift was employed to mitigate the systematic error of overestimating the stability of open-shell configurations in CASPT2.[41] A suitably chosen IPEA parameter is supposed to shift the diagonal elements of the Fock operator, so that the energy denominators assume approximate values of either electron affinity (EA) or ionization potential (IP), depending on whether the excitation is into or from a partially occupied orbital. It was observed that the recommended value of IPEA of 0.25 hartree results in significantly overestimated excitation energies, and consequently a reduced value of 0.10 hartree was adopted. The discrepancy between the recommended value and the applied value in the present case might perhaps be attributed to deficiencies of using the cc-pVDZ basis set for the correlated calculations. In a preliminary study on the 1^1B_{2u}, 1^1B_{1u}, 1^3B_{2u}, and 1^3B_{1u} excited states of benzene, it was observed that the CASSCF-CASPT2/cc-pVDZ (IPEA = 0.10) excitation energies approach the CASSCF-CASPT2/cc-pVTZ (IPEA = 0.25) values on average within 0.10 eV, which is significantly closer than CASSCF-CASPT2/cc-pVDZ with the IPEA of 0.25 hartree retained.

The multireference-based calculations were performed with MOLCAS 6.4,[42] and the time-dependent DFT was performed with the Gaussian 03 quantum chemical suite.[43] The CASSCF transition dipole moments (TDMs) in length representation were calculated employing the RASSI module of MOLCAS.[44] The oscillator strengths f were calculated from the CASSCF TDMs and the CASPT2 vertical excitation energies ΔE (in hartrees) according to

$$f = \frac{2}{3}(\mathrm{TDM})^2 \Delta E \qquad (1)$$

Results and Discussion

A. Geometries. *A.1. Ground State Geometries.* The calculated and experimental[45,46] geometric parameters of DF, TCDF, and OCDF are shown in Table 1.

The X-ray structure of DF[45a] presented in Table 1 is the one improved over an earlier report,[45b] because it was refined by considering an important structural disorder characteristic of DF crystals. The thus-improved set of parameters is in much better agreement with the calculations, in particular for B3P86, and to a somewhat lesser extent for CASSCF.

Being slightly distorted from the plane toward a boat conformation, the crystalline DF is of the mirror (C_s) symmetry, whereby the middle furan ring forms a 1.5° dihedral angle with the benzene rings.[45a] The IR and Raman spectra point to the C_{2v} symmetrical structure in both the solution phase and vapor phase,[18] which is here supported by the vibrational analysis of the C_{2v} optimized minimum (section B). The B3P86 parameters follow closely the relative changes in the C−C bond lengths within the benzene rings, deviating at most 0.005 Å from experiment. This is important in view of some unexpectedly large discrepancies between the B3P86 and X-ray parameters of TCDF (vide infra). CASSCF predicts altogether smaller variations in the C−C bond lengths, thus exhibiting somewhat larger deviations, which peak to 0.011 Å in the case of r_{2CC}. The absolute reliability of the two methods is difficult to assess, however, considering that certain discrepancies should exist between the gas and crystal phase parameters.

With both theoretical approaches the most serious deviations are found for the r_{CO} and r_{7CC} distances within the middle furan ring, which is surprising knowing that B3P86 and B3LYP perform very accurately for the sole furan.[47] The r_{CO} bond length is too short by 0.014 (0.025 Å) via B3P86 (CASSCF). The discrepancies in CASSCF are similar to those seen in dioxins.[27,28] Correlating also the oxygen lone pair by introducing the appropriate virtual orbital (thus creating a (14,14) active space) does not lead to any significant improvement. The additional orbital retains a negligible active occupancy, and consequently the final C−O bond length is increased by only 0.001 Å. The HF/cc-pVTZ optimization results in the similar C−O bond length (1.353 Å), which confirms that the C−O bond remains essentially uncorrelated within the π-type active space, and that the benefits of using larger basis sets would be small. Restoring some of the missing dynamic correlation via B3P86 (Table 1), B3LYP (d(C−O) = 1.376 Å), or MP2/cc-pVDZ (d(C−O) = 1.377 Å) partially resolves the discrepancy. Interestingly, while fully repairing the notably exaggerated C−Cl bond lengths by B3LYP (also seen with dioxins[28]), B3P86 results in the C−O bond shortened by 0.006 Å relative to the B3LYP value, thus deviating somewhat more from the experiment.

The unexpectedly large deviation in r_{7CC}, in particular for the DFT-based methods, is more difficult to rationalize. The MP2/cc-pVDZ and B3LYP/6-31G(d,p) optimizations result in the same r_{7CC} value of 1.454 Å, which is close to that from CASSCF. The discrepancy is all the more surprising knowing that the B3LYP/6-31G(d,p) optimizations of two DF-related compounds, fluorene (CH_2 replaces O) and carbazole (NH replaces O), resulted in 1.470 and 1.450 Å, respectively, for the r_{7CC} equivalent distances, which agrees excellently with the X-ray values of 1.472 and 1.451 Å.[48,49] Thus we suspect that a larger uncertainty might be present in the r_{7CC} X-ray distance of DF.

The changes in the DF skeleton upon introducing the chlorine substituents at the 2, 3, 7, and 8 positions are predicted to be small. For the most part, B3P86 and CASSCF result in similar changes in the bond lengths. The most relevant difference is in the predicted increase in r_{4CC} due to the repulsive interactions between the vicinal Cl atoms. Here CASSCF predicts only a minor elongation of 0.002 Å, whereas B3P86 gives 0.008 Å, which is the largest such change in the structure. The agreement between the B3P86 and X-ray parameters[46] is significantly poorer than in the case of DF, in particular for r_{2CC}, r_{5CC}, and r_{6CC}, which might suggest that crystalline TCDF exhibits a structural disorder similar to that observed in DF. This would render some of the X-ray parameters similarly inaccurate; e.g., by ignoring the disorder in DF, some of the C−C bonds within the benzene rings turned out manifestly too short.[45a]

The X-ray data for the fully chlorinated congener are lacking. The general tendency is that of elongated C−C bond lengths within the benzene rings on average by 0.004 Å relative to DF, with r_{3CC} as the sole exception. On going from DF to OCDF, r_{3CC} exhibits a very slight increase via B3P86, and even a notable decrease via CASSCF. The B3P86 prediction is more trustworthy here, particularly considering that the near-degeneracy effects are comparable in DF, TCDF, and OCDF

TABLE 1: Geometric Parameters of the Ground and Excited States of DF, TCDF, and OCDF at the CASSCF(14,13)/cc-pVDZ and B3P86/6-31G(d,p) Levels

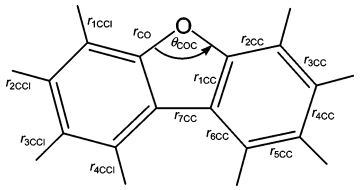

DF

	r_{CO}	r_{1CC}	r_{2CC}	r_{3CC}	r_{4CC}	r_{5CC}	r_{6CC}	r_{7CC}	θ_{COC}
1^1A_1									
CASSCF	1.359	1.399	1.391	1.397	1.407	1.395	1.401	1.458	106.6
B3P86	1.370	1.404	1.385	1.392	1.401	1.390	1.396	1.447	106.0
exptl[a]	1.384	1.399	1.380	1.388	1.400	1.388	1.398	1.438	105.5
$\pi-\pi^*$ (CASSCF)									
2^1A_1	1.350	1.437	1.393	1.422	1.416	1.423	1.415	1.422	108.6
1^1B_2	1.366	1.423	1.400	1.417	1.422	1.417	1.420	1.426	105.9
2^1B_2	1.355	1.442	1.367	1.430	1.416	1.391	1.445	1.386	107.1
1^3A_1	1.353	1.381	1.427	1.426	1.387	1.439	1.428	1.456	106.0
1^3B_2	1.364	1.450	1.358	1.447	1.419	1.384	1.452	1.379	107.4

TCDF

	r_{CO}	r_{1CC}	r_{2CC}	r_{3CC}	r_{4CC}	r_{5CC}	r_{6CC}	r_{7CC}	r_{2CCl}	r_{3CCl}	θ_{COC}
1^1A_1											
CASSCF	1.356	1.397	1.387	1.396	1.409	1.394	1.396	1.457	1.738	1.740	106.4
B3P86	1.368	1.403	1.381	1.393	1.409	1.390	1.392	1.445	1.730	1.734	105.8
exptl[b]	1.385	1.394	1.366	1.387	1.404	1.380	1.381	1.448	1.725	1.732	105.7
$\pi-\pi^*$ (CASSCF)											
2^1A_1	1.348	1.434	1.390	1.421	1.419	1.423	1.411	1.421	1.734	1.734	108.4
1^1B_2	1.363	1.419	1.396	1.416	1.426	1.417	1.417	1.426	1.732	1.733	105.8
2^1B_2	1.353	1.439	1.364	1.431	1.421	1.389	1.441	1.385	1.726	1.740	107.0
1^3A_1	1.350	1.379	1.424	1.426	1.387	1.440	1.422	1.455	1.737	1.736	105.9
1^3B_2	1.361	1.447	1.355	1.448	1.423	1.381	1.448	1.379	1.728	1.740	107.2

OCDF

	r_{CO}	r_{1CC}	r_{2CC}	r_{3CC}	r_{4CC}	r_{5CC}	r_{6CC}	r_{7CC}	r_{1CCl}	r_{2CCl}	r_{3CCl}	r_{4CCl}	θ_{COC}
1^1A_1													
CASSCF	1.340	1.400	1.391	1.390	1.415	1.403	1.416	1.488	1.725	1.727	1.734	1.727	106.8
B3P86	1.353	1.407	1.386	1.393	1.410	1.404	1.410	1.471	1.717	1.718	1.724	1.720	106.1
$\pi-\pi^*$ (CASSCF)													
2^1A_1	1.334	1.441	1.389	1.419	1.418	1.438	1.425	1.444	1.722	1.724	1.727	1.721	108.9
1^1B_2	1.348	1.427	1.396	1.415	1.427	1.433	1.431	1.457	1.722	1.722	1.726	1.722	106.3
2^1B_2	1.336	1.447	1.365	1.429	1.418	1.400	1.460	1.408	1.724	1.717	1.734	1.712	107.4
1^3A_1	1.336	1.383	1.424	1.423	1.389	1.452	1.441	1.480	1.715	1.728	1.729	1.718	106.3
1^3B_2	1.345	1.455	1.356	1.444	1.421	1.395	1.469	1.403	1.725	1.718	1.733	1.721	107.5

[a] Experimental geometry from the X-ray data.[45a] [b] Experimental geometry from the X-ray data.[46]

(the corresponding active occupancies are quite similar), which leaves chiefly the dynamic correlation effects to decide on the geometric parameters. The largest elongation is that exhibited by r_{7CC} (0.030 and 0.024 Å via CASSCF and B3P86), which is due to the essentially single character of the 7CC bond and the pronounced repulsion between the Cl atoms at the 1 and 9 positions. These atoms are only 3.2 Å apart, which is considerably smaller than the sum of their van der Waals radii (1.8 Å + 1.8 Å = 3.6 Å). The most interesting feature is the considerably shortened C−O bond, the effect that was also observed to a similar extent in the longitudinally polychlorinated dioxins (positions 1, 4, 6, and 9).[28] This, together with the trends in the nearby bonds (r_{2CC} about the same or slightly elongated, r_{1CCl} notably shorter than the C−Cl bonds in TCDF), is indicative of the cis effect,[50] usually recognized in the context of alkenes, which are 1,2-disubstituted by highly electronegative atoms. As a result, the cis configurations may surprisingly become more stable than the trans. The bend of the electron density from the C═C bond axis toward the region between the electronegative substituents[50] (here, the O and Cl atoms) then brings about changes in the nearby bond lengths analogous to those observed here.

A.2. Excited State Geometries. The changes in the structural parameters in the excited states of DFs reflect faithfully the redistribution of the electronic density upon excitations, as can be deduced from Table 2, which shows the leading configurations in the CASSCF configuration interaction (CI) expansions in DF (please, refer also to the pictures of the active orbitals within the Supporting Information).

The CI configurations dominating the excited states of the remaining two congeners are completely analogous to those of DF (Table 2). As a result, the equivalent excited states exhibit very similar patterns of changes in bond lengths relative to the corresponding ground state. The invariably observed feature in the five excited states is that of the shortened r_{7CC} distance, sometimes considerably as in the 2^1B_2 and 1^3B_2 states, where this bond displays essentially a double character. This is a direct consequence of the lowest unoccupied molecular orbital (LUMO; b_1 symmetry) incorporating the 7CC π-bonding interaction, and thus the effect most noticeably tells in the B_2 states, which

TABLE 2: Dominant Configurations (Weight in the CI Expansion >0.10) in the CASSCF Wave Functions of DF at Optimized Geometries

	singlets			triplets		
state	b_1	a_2	weight	b_1	a_2	weight
$1A_1$	2222000	222000	0.79	2221100	222000	0.47
				2222000	212100	0.28
$2A_1$	2221100	222000	0.39			
	2222000	221100	0.22			
$1B_2$	2222100	221000	0.41	2222100	221000	0.70
	2222010	212000	0.14			
$2B_2$	2222100	221000	0.68			

TABLE 3: CASSCF(14,13)/cc-pVDZ and B3P86/6-31G(d,p) Harmonic Vibrational Wavenumbers (cm^{-1}) of the Ground ($^1A_1$) State of DF[a,b]

a_1			a_2			b_1			b_2		
CASSCF	B3P86	exptl	CASSCF	B3P86	exptl	CASSCF	B3P86	exptl	CASSCF	B3P86	exptl
215	216	217	149	150	150	102	107	103	516	513	516
420	423	424	281	291	287	311	312	310	555	552	556
656	656	660	429	441	440	417	421	419	616	610	617
738	744	746	552	568	576	545	562	562	849	851	849
858	846	850	711	737		697	717	724	993	1000	1005
999	1020	1010	737	754	769	721	748	752	1022	1024	1024
1094	1103	1103	812	846	855	811	846	849	1107	1115	1114
1120	1147	1148	887	917	931	887	917	930	1129	1155	1153
1188	1200	1170	924	955	967	926	956	967	1221	1218	1201
1249	1262	1245							1261	1279	1286
1290	1312	1309							1302	1369	1319
1324	1387	1348							1467	1463	1457
1466	1457	1448							1495	1483	1477
1506	1504	1495							1606	1612	1593
1605	1622	1595							1618	1630	1599
1657	1662	1636							3101	3126	3048
3101	3126	3040							3113	3135	3061
3114	3136	3061							3125	3147	3074
3126	3148	3082							3137	3160	3096
3138	3160	3096									

[a] The wavenumbers are scaled by factors of 0.9293 (CASSCF)[28] and 0.9759 (B3P86).[51] [b] Experimental wavenumbers from the vapor, liquid, and solid IR and Raman spectra.[18]

always include the transfer of electron density from the a_2 occupied (necessarily π_{7CC}* in character) to the b_1 virtual MOs. Table 2 furthermore reveals that the singlets and triplets within the same space symmetry differ significantly with respect to the dominant configurations (e.g., 2^1A_1 and 1^3A_1 or 1^1B_2 and 1^3B_2), which shows in dissimilar trends in the geometric parameters of the corresponding minima. This contrasts the situation in dioxins, where singlets and triplets within a given symmetry species are typically much more alike.[28]

In DF a conformational similarity between the ground and the first excited state equilibria is reflected in the strong 0_0^0 origin[22,23] and the similar rotational constants. The agreement between the CASSCF and experimental[22] (in parentheses) rotational constants is very rewarding: 0.0765 (0.0760 cm^{-1}), 0.0200 (0.0200 cm^{-1}), and 0.0159 (0.0159 cm^{-1}) for the 1^1A_1 structure, and 0.0752 (0.0753 cm^{-1}), 0.0198 (0.0198 cm^{-1}), and 0.0157 (0.0157 cm^{-1}) for the 2^1A_1 structure, as obtained via the SA-CASSCF optimization.

B. Harmonic Wavenumbers. The CASSCF and B3P86 harmonic wavenumbers of DF, TCDF, and OCDF are presented in Tables 3, 4 and 5, respectively. The wavenumbers are scaled by the recommended factor of 0.9759 for the B3P86/6-31G(d,p) level[51] and a tentative factor of 0.9293 for the CASSCF, which minimized the differences between the experimental and calculated wavenumbers in three polychlorinated dioxins.[28] Whereas the vibrational spectrum of DF received considerable attention in the past,[13,18] which resulted in a near-definite assignment of the majority of fundamental modes (Table 3), studies and assignments of spectra of TCDF and OCDF are to our knowledge still lacking, despite the fact that, equally for dioxins, a reliable distinguishing between the similar IR spectra would be crucial for identification and separation of the DF congeners.

The chlorination considerably reduces the force constants of a large majority of modes, decreasing the zero-point vibrational energies (ZPVEs) by roughly 100 kJ mol^{-1} per four introduced chlorine substituents: the B3P86 ZPVEs equal 424 (experimental[18] 420 kJ mol^{-1}), 322, and 225 kJ mol^{-1} for DF, TCDF, and OCDF, respectively. The CASSCF wavenumbers are generally smaller than the B3P86 ones, with the corresponding CASSCF ZPVEs equaling 419, 320, and 222 kJ mol^{-1}. The agreement between the measured and calculated fundamentals of DF is very good, in particular for B3P86 (Table 3). A doubtful experimental assignment (890 cm^{-1})[18] within the a_2 modes is all the more questioned by the present calculations, and so the corresponding entry is left blank in Table 3. Omitting this, together with the C−H stretching modes (>3000 cm^{-1}) on account of the significantly larger experimental uncertainties,[18] the averages (observed − calculated) and the root-mean-square deviations (rmsd) (in parentheses) for the scaled CASSCF and B3P86 wavenumbers equal 9.0 (19.0 cm^{-1}) and −3.8 (14.0 cm^{-1}), respectively. These values can be compared to −1.4 (13.6 cm^{-1}) obtained via the semiempirical (AM1) scaled quantum mechanical force field employing the bicyclic scale factors (SQM-BSF-AM1). Thus, the B3P86 and SQM-BSF-AM1 force fields are of comparable accuracy, while CASSCF deviates somewhat more, similar to the findings for dioxins.[28] It should be noted, however, that neither CASSCF nor B3P86 exhibits

TABLE 4: CASSCF(14,13)/cc-pVDZ and B3P86/6-31G(d,p) Harmonic Vibrational Wavenumbers (cm^{-1}) of the Ground ($^1A_1$) State of TCDF[a]

a_1		a_2		b_1		b_2	
CASSCF	B3P86	CASSCF	B3P86	CASSCF	B3P86	CASSCF	B3P86
102	106	54	61	45	56	201	196
191	187	142	150	125	136	249	248
256	254	238	253	248	265	397	393
343	342	370	399	370	387	450	446
484	480	424	446	428	446	585	581
642	640	599	661	591	646	668	664
726	720	714	759	684	724	705	694
803	795	818	871	822	874	926	916
941	927	843	896	839	889	1048	1031
1105	1088					1109	1087
1142	1167					1167	1199
1206	1211					1228	1215
1230	1256					1251	1286
1293	1299					1396	1378
1406	1390					1471	1435
1492	1454					1584	1557
1583	1570					1619	1587
1660	1625					3144	3112
3146	3112					3159	3128
3159	3128						

[a] The wavenumbers are scaled by factors of 0.9293 (CASSCF)[28] and 0.9759 (B3P86).[51]

TABLE 5: CASSCF(14,13)/cc-pVDZ and B3P86/6-31G(d,p) Harmonic Vibrational Wavenumbers (cm^{-1}) of the Ground ($^1A_1$) State of OCDF[a]

a_1		a_2		b_1		b_2	
CASSCF	B3P86	CASSCF	B3P86	CASSCF	B3P86	CASSCF	B3P86
104	100	4i	8	36	37	172	172
172	172	52	54	74	78	206	203
221	218	79	82	98	100	226	224
255	253	172	175	219	225	241	238
267	268	329	347	292	304	329	330
344	349	379	395	384	399	349	348
359	360	560	596	544	576	468	473
479	478	605	633	600	630	580	576
654	657	742	718	693	700	712	708
730	741					782	783
819	816					846	849
944	952					1018	1009
988	987					1108	1108
1122	1188					1144	1264
1211	1264					1275	1307
1264	1313					1353	1350
1399	1378					1437	1415
1421	1422					1557	1543
1558	1554					1577	1585
1619	1625						

[a] The wavenumbers are scaled by factors of 0.9293 (CASSCF)[28] and 0.9759 (B3P86).[51]

the large error in the b_1 fundamental at 752 cm^{-1}, which SQM-BSF-AM1 strangely overshoots by 43 cm^{-1},[18] and that both methods clearly suspect the above-mentioned tentative a_2 assignment.

The modes pertaining to the motions in the molecular plane (a_1 and b_2) generally agree closely between CASSCF and B3P86, whereas the out-of-plane modes (a_2 and b_1) exhibit somewhat larger discrepancies, with the CASSCF wavenumbers being consistently smaller than the B3P86. The reason may be that the out-of-plane modes, especially those involving the ring-puckering motions, include disruption of the electron delocalization via conjugation throughout the three rings. Because of the missing dynamic correlation in CASSCF, the stabilizing effect of conjugation is underestimated, which makes the CASSCF force constants smaller. This effect also tells in the context of the CASSCF equilibrium geometry of OCDF (vide infra). In all three congeners a host of the out-of-plane modes appears in quasi-degenerate (a_2, b_1) pairs. This is most visible in the parent DF, and is least expressed in OCDF, where energies required for the in-phase and out-of-phase waggings differ more, owing to the large repelling chlorine substituents.

The most prominent absorption in the low-frequency region of the DF spectrum[18] appears as a split intense band due to the two near-lying b_1 fundamentals at 724 and 752 cm^{-1} (Table 3). These modes correspond to the out-of-plane in-phase wagging of the H atoms strongly coupled to the puckering of the middle furan ring. The higher frequency mode is predicted to be the second most intense, with the intensity exceeding 100 km mol^{-1}. Owing to the large change in the nature of substituents, the corresponding region in TCDF and OCDF is largely darkened, particularly in OCDF, where no b_1 mode has a noteworthy intensity.

By far the strongest band in all three compounds, well exceeding 250 km mol^{-1} in TCDF and OCDF, belongs to the b_2 symmetry and appears around 1200, 1450, and 1350 cm^{-1} in DF, TCDF, and OCDF, respectively (Tables 3, 4, and 5).

TABLE 6: Singlet Excitation Energies (Vertical T_v and Adiabatic T_0 in eV) at the Single-State CASSCF/CASPT2(14,13)/cc-pVDZ and TD-B3P86/6-31G(d,p) Levels

	DF				TCDF			OCDF		
	CASPT2[a]				CASPT2[a]			CASPT2[a]		
state	T_v	T_0	TD-B3P86 T_v	exptl T_0	T_v	T_0	TD-B3P86 T_v	T_v	T_0	TD-B3P86 T_v
2^1A_1	4.36	4.16	4.56	4.1714[b]	4.23	4.03	4.26	4.08	3.86	3.95
1^1B_2	4.72	4.51	4.75		4.54	4.28	4.32	4.51	4.26	4.25
2^1B_2	5.16	4.94	5.41		4.90	4.67	5.08	4.56	4.22	4.43
3^1A_1	5.98		5.63		5.79		5.21	5.74		5.08
1^1A_2							5.57			4.89
1^1B_1							5.56			4.94
2^1B_1							5.85			5.02
2^1A_2							5.84			5.08
4^1A_1	6.40		6.15		6.19		5.54	6.11		5.19
3^1B_2	6.41		5.76		6.20		5.41	5.98		5.06
4^1B_2	6.55		6.13		6.22		5.64	6.08		5.41
5^1B_2	6.58		6.57		6.39			6.18		
6^1B_2	6.71		7.03		6.55			6.19		
5^1A_1	6.77		6.34		6.62		5.94	6.57		
6^1A_1	7.42		6.54		7.22		6.04	6.59		5.36
3^1B_1							6.06			5.58
3^1A_2							6.08			5.64

[a] The IPEA level shift parameter of 0.10 hartree combined with the imaginary level shift parameter of 0.10 hartree. [b] Experimental excitation energy from sub-Doppler high-resolution laser excitation spectroscopy.[22,23]

The corresponding mode is best described as the asymmetric C−O stretch strongly coupled to the in-plane waggings of the H atoms in DF and TCDF. This band can be observed as analogous to the extremely strong dioxin fundamental residing around 1500 cm^{-1}.[28] However, in DFs it is on average 5 times less intense, is clearly red-shifted, and appears more prone to frequency shifts in different congeners. Because these fundamentals most distinctly reflect the differences between the dibenzofuran and dioxin skeletons, this should make them a feature of the foremost analytical value in distinguishing between these classes of pollutants.

The lowest frequency mode of the a_2 symmetry of OCDF is exceedingly small by B3P86, and even becomes imaginary by CASSCF, meaning that the true CASSCF minimum is a C_2 symmetrical one. This mode most importantly corresponds to the out-of-phase out-of-plane wagging of the two Cl atoms closest to each other (positions 1 and 9), and thus reflects a tendency toward reducing the electrostatic repulsion between the two atoms, whose distance is notably smaller than the sum of their van der Waals radii (vide supra). This comes at the expense of deviating from the planar structure, and consequently disrupting the conjugation. The corresponding CASSCF and B3P86 wavenumbers of 4i and 8 cm^{-1}, respectively (Table 5), point to a remarkably flat potential, and in the case of CASSCF only a slight deviation from the plane in what would be the true minimum. This is reminiscent of the mild symmetry breaking along the butterfly mode in the longitudinally polychlorinated dioxins.[28] This issue was previously attributed to the missing dynamic correlation in CASSCF, whereby the benefits of stabilization via conjugation delocalization are probably underestimated, and the purely electrostatic effects are given more weight.[28] However, the overall effect on the CASSCF geometric parameters, vibrational wavenumbers, and electronic transitions should be very small, estimating from similar effects due to the butterfly motion in dioxins.[28]

The lowest frequency modes within the b_1 symmetry (Tables 3−5) correspond to the butterfly-like distortion of the dibenzofuran skeleton. Although very small, particularly in TCDF and OCDF, the corresponding wavenumbers are still roughly 5 times larger than in the analogous dioxins,[28] which is due to the impeded mobility of the DF skeleton, specifically of the middle furan ring, which has to assume an envelope conformation. Because the butterfly mode is coupled to the stretching of mainly the lateral C−H (C−Cl) bonds, the trend of diminishing wavenumbers with the increased number of chlorine atoms is visible, and is in a relative sense very similar to that observed in dioxins; e.g., in TCDF (2,3,7,8-TCDD)[28] the wavenumber is roughly 2 times smaller than in DF (DD).[27]

C. Electronic Transitions. In Tables 6 and 7 the calculated CASSCF/CASPT2 and TD-B3P86 singlet and triplet excitation energies of DF, TCDF, and OCDF are shown and compared with the available experimental data. The CASSCF and TD-B3P86 oscillator strengths in the length representation are given in Table 8. The experimental UV spectra supplemented by the CASSCF/CASPT2 vertical rules are presented in Figures 2−4.

Both CASSCF/CASPT2 and TD-B3P86 predict $2^1A_1 \leftarrow 1^1A_1$ as the lowest lying transition in all three congeners. In the case of DF, this gives rise to the $S_1 \leftarrow S_0$ band, whose ro−vibrational features were studied in detail via ultrahigh-precision sub-Doppler laser spectroscopy.[22,23] The CASSCF/CASPT2 adiabatic excitation energy of 4.16 eV (Table 6) agrees remarkably well with the intense 0_0^0 origin observed at 4.1714 eV.[23] Such a close agreement gives the present theoretical approach a valuable credit, especially considering that similar high-precision experiments are still lacking for the toxic chlorinated derivatives. The optimal excitation wavelengths utilized in the luminescence experiments[9] on DF (246 nm (5.05 eV) and 285 nm (4.35 eV)) and TCDF (257 nm (4.82 eV) and 307 nm (4.04 eV)) can be readily associated with the $2^1B_2 \leftarrow 1^1A_1$ and $2^1A_1 \leftarrow 1^1A_1$ CASSCF/CASPT2 vertical excitation energies (Table 6). The room-temperature fluorescence maxima, 316 nm (3.92 eV) in DF and 340 nm (3.65 eV) in TCDF,[9] are reasonably reproduced if the vertical emission is simulated by calculating the 1^1A_1 state in the 2^1A_1 equilibrium geometry. The result is the reduced energy differences with respect to the 2^1A_1 minima, 4.03 and 3.89 eV for DF and TCDF, respectively, which are now much closer to the fluorescence maxima.

Much earlier Bree et al. carried out a detailed investigation of the UV absorptions in DF analyzing the vapor, solution, powder, and polarized crystal state spectra.[14] Their efforts led to an assignment of symmetry labels to six band systems

TABLE 7: Triplet Excitation Energies (Vertical T_v and Adiabatic T_0 in eV) at the Single-State CASSCF/CASPT2(14,13)/cc-pVDZ and TD-B3P86/6-31G(d,p) Levels

	DF				TCDF				OCDF		
	CASPT2[a]		TD-B3P86		CASPT2[a]		TD-B3P86		CASPT2[a]		TD-B3P86
state	T_v	T_0	T_v	exptl[b]	T_v	T_0	T_v	exptl[b]	T_v	T_0	T_v
1^3B_2	3.61	3.23	3.20	3.05; 2.97	3.49	3.10	3.01	2.63	3.44	3.08	2.90
1^3A_1	4.16	3.84	3.72		4.06	3.76	3.52		3.80	3.45	3.20
2^3A_1	4.38		4.27		4.22		3.98		4.13		3.86
2^3B_2	4.39		4.25		4.23		3.95		4.10		3.77
3^3B_2	4.78		4.66		4.64		4.38		4.55		4.02
3^3A_1	4.85		4.66		4.71		4.33		4.61		4.28
4^3A_1	5.01		5.00		4.86		4.73		4.67		4.33
4^3B_2	5.56		5.13		5.40		4.88		5.36		4.69
1^3A_2							5.21				4.63
1^3B_1							5.22				4.68
2^3A_2							5.63				4.83
2^3B_1							5.68				4.80
5^3B_2	6.39		5.93		6.31		5.57		6.20		5.16
5^3A_1	6.82		5.98		6.68		5.49		6.64		5.23
6^3B_2	6.90		6.29		6.78				6.56		
6^3A_1	7.12		6.07		7.00		5.68		6.85		

[a] The IPEA level shift parameter of 0.10 hartree combined with the imaginary level shift parameter of 0.10 hartree. [b] Experimental energies from the room-temperature phosphorescence maxima.[9,17]

TABLE 8: CASSCF(14,13)/cc-pVDZ and TD-B3P86/6-31G(d,p) Oscillator Strengths in the Length Representation

	DF		TCDF		OCDF	
	CASSCF[a]	TD-B3P86	CASSCF[a]	TD-B3P86	CASSCF[a]	TD-B3P86
$2^1A_1 \leftarrow 1^1A_1$	0.0094	0.0257	0.0090	0.0180	0.0161	0.0593
$3^1A_1 \leftarrow 1^1A_1$	0.0966	0.0765	0.0878	0.0704	0.0866	0.1750
$4^1A_1 \leftarrow 1^1A_1$	0.0042	0.0121	0.0047	0.0005	0.0143	0.0409
$5^1A_1 \leftarrow 1^1A_1$	0.0154	0.0840	0.0153	0.1351	0.0064	0.0240
$6^1A_1 \leftarrow 1^1A_1$	0.0067	0.0052	0.0042	0.0131	0.0076	
$1^1B_2 \leftarrow 1^1A_1$	0.0599	0.2866	0.0623	0.4614	0.0365	0.3985
$2^1B_2 \leftarrow 1^1A_1$	0.3059	0.0270	0.3103	0.0670	0.2472	0.0010
$3^1B_2 \leftarrow 1^1A_1$	0.2898	0.3549	0.2419	0.5669	0.6337	0.4213
$4^1B_2 \leftarrow 1^1A_1$	0.5524	0.3399	0.6345	0.1900	0.2814	0.5169
$5^1B_2 \leftarrow 1^1A_1$	0.2606	0.0821	0.0020		0.2169	
$6^1B_2 \leftarrow 1^1A_1$	0.0317	0.4495	0.2878		0.1567	

identified in the 200−330 nm region. Earlier reported barely visible system I,[11] to be observed near 3.90 eV, is definitely proved too low in energy by our calculations, and is probably an artifact due to impurities as was also suspected by Bree et al.[14] System II originating at 4.17 eV corresponds to an $^1A_1 \leftarrow {}^1A_1$ band, and system III with the maximum at ∼4.4 eV (∼280 nm, Figure 2) corresponds to a $^1B_2 \leftarrow {}^1A_1$ band, based on the symmetry assignments from the single-crystal spectra. This sequence of transitions is now confirmed by the calculations. The CASSCF/CASPT2 1^1A_1 and 1^1B_2 adiabatic excitation energies (Figure 2) are very close to the two sharp maxima within the systems II and III, which indicates that the 1^1B_2 band might also have a very strong 0_0^0 origin, even stronger than the 2^1A_1 has. Overall, the calculations suggest that the $2^1A_1 \leftarrow 1^1A_1$ and $1^1B_2 \leftarrow 1^1A_1$ band systems are solely responsible for the absorptions in the broad intense 260−300 nm region. Therefore, some surprisingly strong transitions within the former band should be explained in terms of a very efficient mechanism of vibronic intensity borrowing from the latter, and not by yet another transition present in the region, which was proposed as an alternative.[14] That is, earlier[15] as well as very recent experimental studies[22,23] confirmed that a host of transitions to the first vibrational levels of the b_2 modes of the 2^1A_1 state, most prominently 55_0^1 (observed at $0_0^0 + 443$ cm^{-1}),[23] gain remarkably in intensity via vibronic coupling with the near-lying 1^1B_2 state. Here TD-B3P86 (Table 6) confirmed that no transition other than the $\pi-\pi^*$ type emerges in the observed UV region, which contradicts some previous conjectures.[10,52]

A region of low absorption (Figure 2) separates systems II and III from system IV, which is characterized by the sharp maximum at 4.98 eV and assigned as another $^1B_2 \leftarrow {}^1A_1$ transition.[14] This corresponds to the calculated $2^1B_2 \leftarrow 1^1A_1$. Here CASSCF, unlike TD-B3P86, correctly predicts a much stronger intensity than those of the preceding two transitions (Table 8). In both DF and TCDF the sharp maxima are regularly red-shifted by ca. 5 nm from the vertical, and blue-shifted from the CASSCF/CASPT2 adiabatic excitation energies (Figures 2 and 3). Two more systems, denoted V and VI, were observed in the higher frequency region (200−230 nm), which would correspond to the calculated moderately intense $3^1A_1 \leftarrow 1^1A_1$ (207 nm) and the very strong $3^1B_2 \leftarrow 1^1A_1$ (193 nm) band systems (Table 8). Here our calculations confirmed the tentative assignment of system V to an A_1 and system VI to a B_2-type transition.[14]

The spectra of TCDF and particularly OCDF are more complex (Figures 3 and 4). The equivalent transitions are red-shifted relative to DF on average by 0.2 eV (0.4 eV) in TCDF (OCDF), with some larger deviations present. Similarly to the spectrum of octachlorodibenzo-*p*-dioxin,[10,28] the spectrum of OCDF[10] (Figure 4) is largely broadened, making it impossible to resolve any finer structures. Because this feature is very much unlike the spectra of DF and TCDF, it was suggested that the rate of intersystem crossing (ISC) increases considerably in the fully chlorinated congener.[10] This is supported by the notably larger phosphorescence yields with increasing chlorination in DFs and dioxins.[9] Our results indicate that the increasing

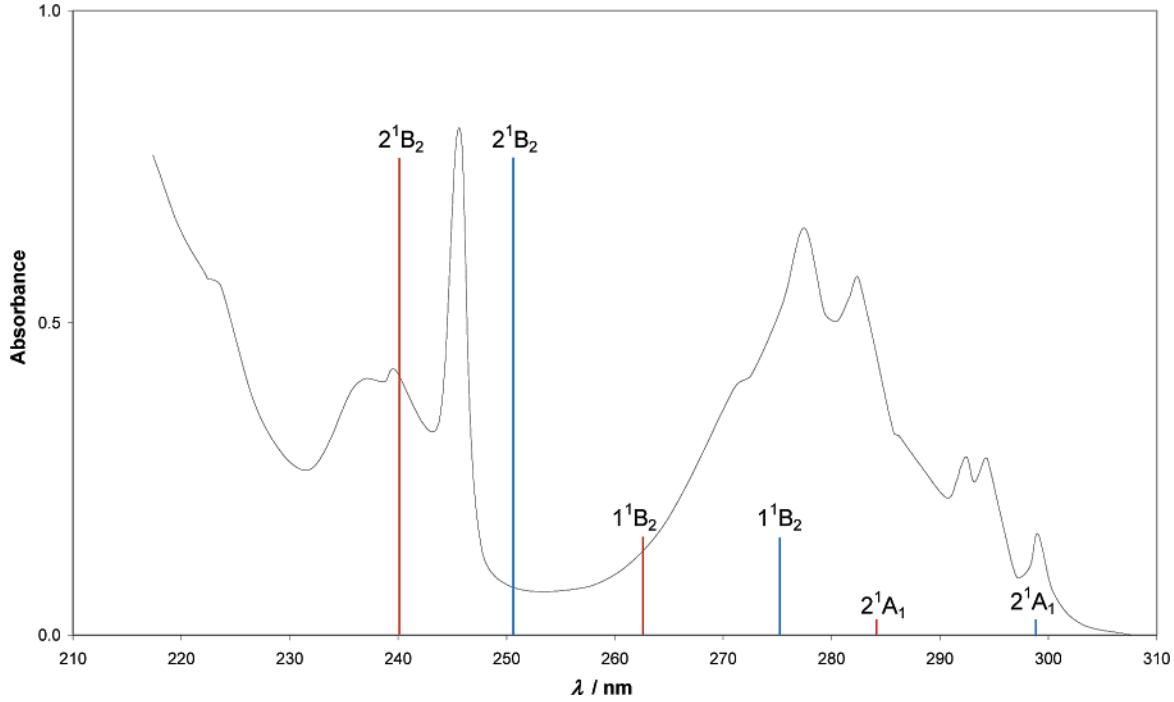

Figure 2. Experimental absorption spectrum of DF ($t \approx 50$ °C)[14] supplemented by the rules denoting the CASSCF/CASPT2 vertical (red) and adiabatic (blue) excitation energies. The heights of the rules are proportionate to the calculated vertical oscillator strengths (Table 8).

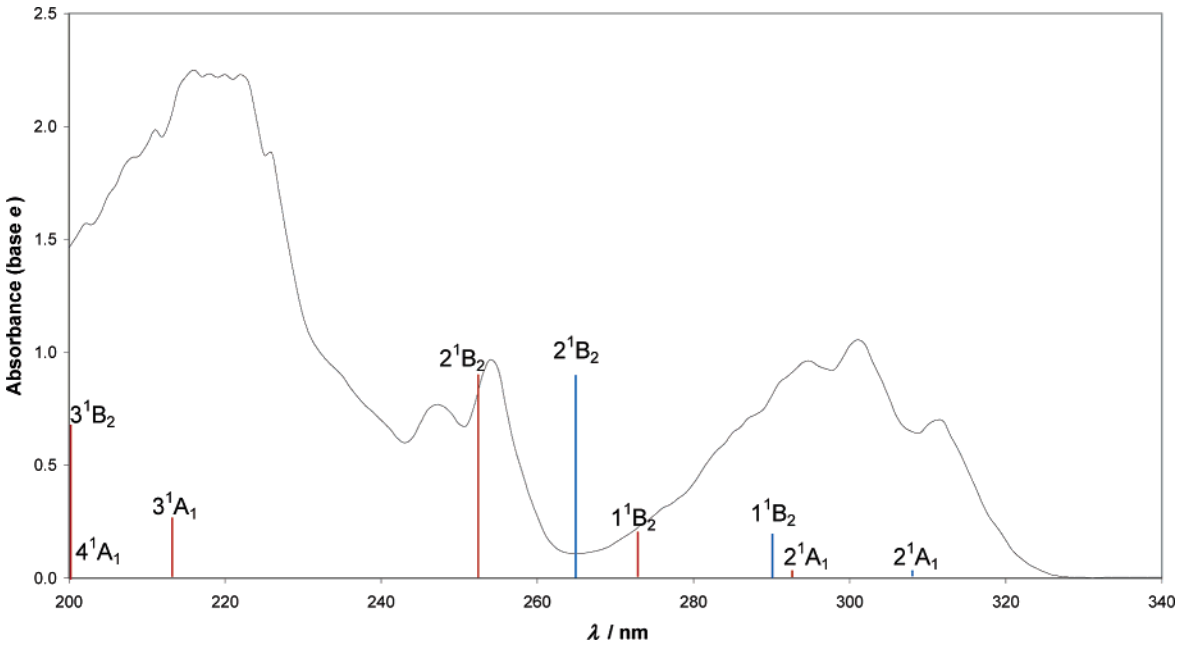

Figure 3. Experimental absorption spectrum of TCDF ($t = 165$ °C)[10] supplemented by the rules denoting the CASSCF/CASPT2 vertical (red) and adiabatic (blue) excitation energies. The heights of the rules are proportionate to the calculated vertical oscillator strengths (Table 8).

complexity of TCDF and OCDF spectra is at least in part due to the progressive crowding of high-intensity spin and symmetry allowed transitions in the 200−220 nm region (Figures 3 and 4).

A poorer reliability of the TD-DFT excitation energies compared to those of CASSCF/CASPT2 was previously established in the case of polychlorinated dioxins,[28] in particular for the higher excited states that approached the threshold roughly set by the Kohn−Sham highest occupied molecular orbital (HOMO) energy criterion.[53] The herein used TD-B3P86 performs quite similarly to TD-B3LYP.[28] By analysis of the orbitals and dominant excitations, it is possible to establish a clear-cut correspondence between the TD-B3P86 and CASSCF $\pi-\pi^*$ states. The second-order correction occasionally reverses the ordering of the CASSCF roots by energy, and consequently, e.g., the 5^1B_2 roots are not equivalent by the dominant excitations in the multiconfigurational and DFT treatments, although the majority of the roots remain so. Whereas for the lower singlet states the agreement with the experiment is still reasonable, albeit inferior to CASSCF/CASPT2, above 5 eV the majority of the TD-B3P86 excitation energies appear drastically underestimated. Consequently, the use of TD-B3P86 was limited to complementing the TCDF and OCDF spectra by indicating the positions of a few additional lower lying states not of the $\pi-\pi^*$ origin. The additional states are either orbitally forbidden (A_2) or confirmed to have negligible to very small intensities (B_1); hence they should have a negligible effect on the appearance of the UV absorption spectra. These states appear

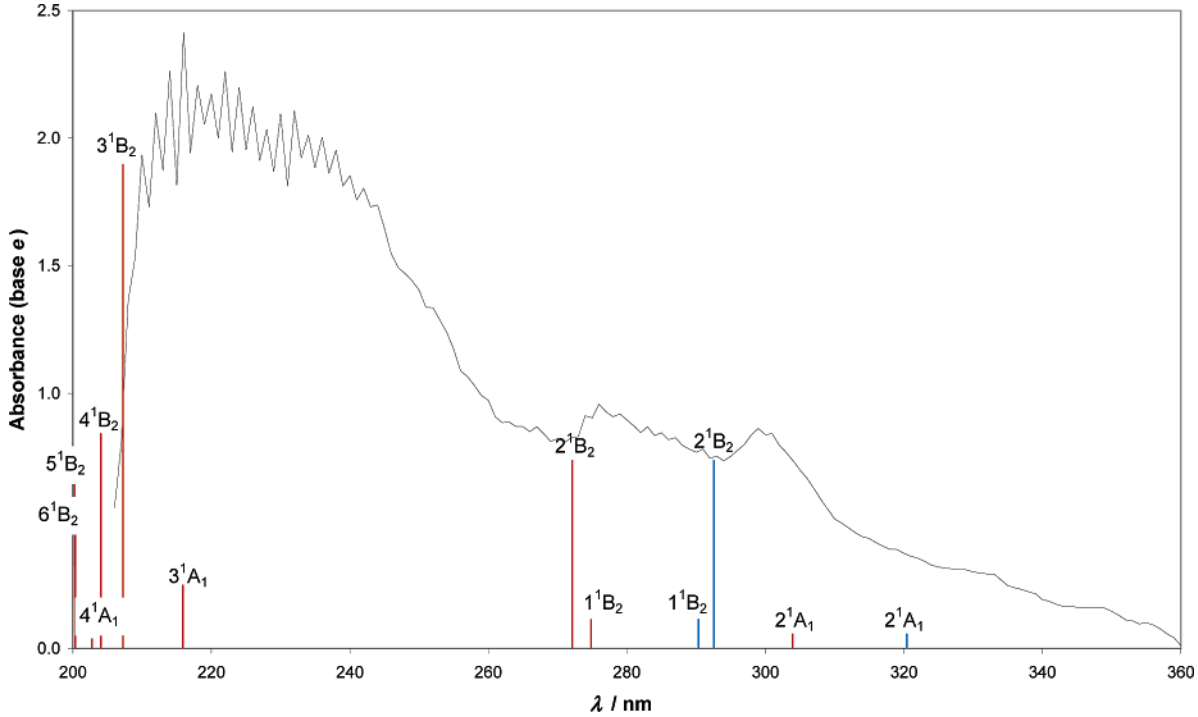

Figure 4. Experimental absorption spectrum of OCDF ($t = 225$ °C)[10] supplemented by the rules denoting the CASSCF/CASPT2 vertical (red) and adiabatic (blue) excitation energies. The heights of the rules are proportionate to the calculated vertical oscillator strengths (Table 8).

in quasi-degenerate A_2-B_1 pairs (Table 6), which reflects the quasi-degeneracies of the orbitals involved in the transitions. The lower lying states (1^1A_2, 2^1A_2, 1^1B_1, and 2^1B_1) are of the $\pi-\sigma_{C-Cl}^*$ origin, whereas excitations from the in-plane chlorine lone pairs ($n_{Cl}-\pi^*$) emerge around 0.2−0.5 eV higher (3^1A_2 and 3^1B_1). Estimating from the discrepancies between the CASSCF/CASPT2 and TD-B3P86 $\pi-\pi^*$ excitation energies in the corresponding energy regions, the lower of these states require on average 0.6−0.8 eV, and the upper more than 1 eV of blue shifting to correspond better to the physical reality. The TD-B3P86 oscillator strengths (Table 8) also show some notable deviations from those of the CASSCF (Table 8), in particular in predicting the 1^1B_2 transition to be much more intense than 2^1B_2, which contradicts the experiment.

Finally, it is of interest to compare the electron spectra to those of dioxins.[27,28] The equivalent excited states are 0.2−0.5 eV higher than in the dioxin analogues. In DFs the singlet B_2 states are generally above the A_1 states in a given energy region, which is contrary to dioxins, where the B_2 equivalent states (B_{3g} and B_{2u}) are always lower than the A_1 equivalent (A_g) states. The reason is that in dioxins the lowest singlet and triplet states are dominated simply by the LUMO ← HOMO excitation, whereas in DFs the strong (LUMO + 1) ← HOMO and LUMO ← (HOMO − 1) configurational mixing dominate the 2^1A_1 states (Table 2), which agrees with the recent CIS calculations.[23] The state dominated exclusively by the LUMO ← HOMO configuration is as high as 2^1B_2. Omission of one of the oxo bridges promotes the conjugation delocalization between the two benzene rings lowering both HOMO and LUMO, and increasing the Kohn−Sham HOMO−LUMO gap by 0.16 eV in DF compared to DD. Interestingly, unlike the singlets, the sequence of the triplet states is identical in DFs and dioxins. The remarkable similarity is reflected even in the quasi-degeneracy of the 2^3A_1 and 2^3B_2 states (Table 7), which correspond to the quasi-degenerate 1^3B_{1u} and 1^3B_{2u} states in dioxins.[27,28]

The 1^3A_1 and 1^3B_2 states retain the C_{2v} symmetry (please, refer to the Supporting Information for the harmonic wavenumbers in the 1^3A_1 and 1^3B_2 minima from Table 1). The experimental energies of the lowest DF and TCDF triplet states (Table 7) originate from the room-temperature phosphorescence maxima, and thus cannot be compared directly to the calculated values, while Shpolskii phosphorescence spectra analogous to those of dioxins[28] are to our knowledge lacking. Still the phosphorescence maxima can be well reproduced, provided the excitation energies are calculated relative to the 1^1A_1 state in the 1^3B_2 minimum geometry, thus simulating vertical emissions. This results in 2.83 and 2.69 eV for DF and TCDF, respectively, which approach the maxima well within the usual CASSCF/CASPT2 error bounds (±0.20 eV[29]).

Conclusions

Multiconfigurational (CASSCF) and density functional theory (B3P86) methods were used in calculating the equilibrium geometries and harmonic vibrational wavenumbers of the ground states of DF, TCDF, and OCDF, while state-averaged CASSCF calculations enabled these properties to be calculated also for several of the lower lying excited states. The electronic transitions in these compounds were studied via combined multireference CASSCF/CASPT2 treatment, as well as the time-dependent DFT (TD-B3P86). From comparison between the calculations and abundant experimental data for the parent DF, it can be deduced that B3P86 results in more reliable equilibrium structures and harmonic wavenumbers than CASSCF, whereas the reliability of CASSCF/CASPT2 is largely superior to TD-B3P86 in predicting the electronic excitation energies. Thus the two approaches complement each other nicely, and the accuracy bounds established for the parent DF are valuable in view of the difficulties in obtaining the experimental data for the toxic chlorinated congeners.

The equilibrium structures of DF and TCDF are of the C_{2v} symmetry, and in the case of B3P86 compare very well to the X-ray parameters. One or two discrepancies are still of dubious origin, because they are absent in related compounds (fluorene and carbazole). This probably indicates that there is a space for

further refinement of the crystal structure of DF and TCDF, particularly in view of the structural disorder inherent to the DF crystals. The OCDF minimum is of the C_{2v} symmetry by B3P86, but relaxes to a C_2 structure by CASSCF via the mode that involves the out-of-phase wagging of the two proximate chlorine atoms. Similarly to the butterfly relaxation observed in longitudinally substituted dioxins, this effect can probably be regarded as an artifact due to the missing dynamic correlation in CASSCF.

The B3P86 wavenumbers compare very favorably to the measured fundamentals, with the exception of a suspiciously assigned a_2 symmetry mode and the high-frequency C−H stretching modes, which themselves have a large experimental uncertainty. Apart from that, the accuracy of the scaled B3P86 is entirely comparable to the SQM tailored force field. The features of the IR spectra that could prove particularly useful in analysis include some low-frequency out-of-plane wagging modes, which differ considerably in intensity between different congeners, as well as the high-intensity band in the 1200−1450 cm^{-1} region corresponding mainly to the C−O asymmetric stretching. While this band has its analogue in dioxins, its appearance, position, and especially intensity should differ considerably between dibenzofuran and dioxin structures.

The equivalent electronic transitions invariably undergo red-shifting with increasing chlorination. The extent of the red shift relative to the parent DF varies in the range of 0.1−0.5 eV in TCDF and 0.2−0.6 eV in OCDF. The lowest transition in all three congeners is $2^1A_1 \leftarrow 1^1A_1$. The experimental band origin and the rotational constants of the 2^1A_1 state agree remarkably well with the CASSCF/CASPT2 predictions in case of the parent DF. The comparison of the electron transitions in DFs and dioxins revealed certain dissimilarities in the ordering and origin of the singlet states and a great analogy of the triplet states.

Acknowledgment. This work was supported by the Ministry of Science and Technology of the Republic of Croatia under Project No. 0098033.

Supporting Information Available: A pictorial representation of the (14,13) active space and Kohn−Sham orbitals of DF, tables of the harmonic vibrational wavenumbers of the 1^1B_2 state of DF, TCDF, and OCDF, and 1^3A_1 and 1^3B_2 states of DF. This material is available free of charge via the Internet at http://pubs.acs.org.

References and Notes

(1) Schecter, A.; Fürst, P.; Fürst, C.; Päpke, O.; Ball, M.; Ryan, J. J.; Cau, H. D.; Dai, L. C.; Quynh, H. T.; Cuong, H. Q.; Phuong, N. T. N.; Phiet, P. H.; Beim, A.; Constable, J.; Startin, J.; Samedy, M.; Seng, Y. K. *Environ. Health Perspect.* **1994**, *102* (Suppl. 1), 159.

(2) Van den Berg, M.; Birnbaum, L.; Bosveld, A. T. C.; Brunström, B.; Cook, P.; Feeley, M.; Giesy, J. P.; Hanberg, A.; Hasegawa, R.; Kennedy, S. W; Kubiak, T.; Larsen, J. C.; van Leeuwen, F. X.; Liem, A. K. D.; Nolt, C.; Peterson, R. E.; Poellinger, L.; Safe, S.; Schrenk, D.; Tillitt, D.; Tysklind, M.; Younes, M.; Wærn, F.; Zacharewski, T. *Environ. Health Perspect.* **1998**, *106*, 775.

(3) Atkinson, R. Atmospheric chemistry of PCBs, PCDDs, and PCDFs. In *Chlorinated Organic Micropollutants: Issues in Environmental Science and Technology*; Hester, R. E., Harrison, R. M., Eds.; The Royal Society of Chemistry: Cambridge, 1996.

(4) Lofroth, G.; Zebuhr, Y. *Bull. Environ. Contam. Toxicol.* **1992**, *48*, 789.

(5) (a) Yoneda, K.; Ikeguchi, T.; Yagi, Y.; Tamade, Y.; Omori, K. *Chemosphere* **2002**, *46*, 1309. (b) Kumagai, S.; Koda, S.; Miyakita, T.; Yamaguchi, H.; Katagi, K.; Yasuda, N. *Occup. Environ. Med.* **2000**, *57*, 204. (c) Lemieux, P. M.; Lutes, C. C.; Abbott, J. A.; Aldous, K. M. *Environ. Sci. Technol.* **2000**, *34*, 377.

(6) (a) *Sax's Dangerous Properties of Industrial Materials*, 10th ed.; Lewis, R. J., Sr., Ed.; Wiley: New York, 2000; Vols. 1−3.

(7) Shepard, B. M.; Young, A. L. In *Human and Environmental Risks of Chlorinated Dioxins and Related Compounds*; Tucker, R. E., Young, A. L., Gray, A. P., Eds.; Plenum Press: New York, 1983.

(8) (a) Schutte, C. J. H.; Bertie, J. E.; Bunker, P. R.; Hougen, J. T.; Mills, I. M.; Watson, J. K. G.; Winnewisser, B. P. *Pure Appl. Chem.* **1997**, *69*, 1633. (b) Schutte, C. J. H.; Bertie, J. E.; Bunker, P. R.; Hougen, J. T.; Mills, I. M.; Watson, J. K. G.; Winnewisser, B. P. *Pure Appl. Chem.* **1997**, *69*, 1641.

(9) Khasawneh, I. M.; Winefordner, J. D. *Talanta* **1988**, *35*, 267.

(10) Funk, D. J.; Oldenborg, R. C.; Dayton, D.-P.; Lacosse, J. P.; Draves, J. A.; Logan, T. *J. Appl. Spectrosc.* **1995**, *49*, 105.

(11) Pinkham, C. A.; Wait, S. C. *J. Mol. Spectrosc.* **1968**, *27*, 326.

(12) Momicchioli, F.; Rastelli, A. *J. Chem. Soc. B* **1970**, 1353 and references therein.

(13) Bree, A.; Vilkos, V. V. B.; Zwarich, R. *J. Mol. Spectrosc.* **1973**, *48*, 124.

(14) Bree, A.; Vilkos, V. V. B.; Zwarich, R. *J. Mol. Spectrosc.* **1973**, *48*, 135.

(15) Bree, A.; Lacey, A. R.; Ross, I. G.; Zwarich, R. *Chem. Phys. Lett.* **1974**, *26*, 329.

(16) Taliani, C.; Bree, A.; Zwarich, R. *J. Phys. Chem.* **1984**, *88*, 2357.

(17) (a) von Borczyskowski, C.; Seiff, F.; Stehlik, D. *J. Phys. Chem.* **1987**, *91*, 327. (b) González, M. A.; López, M. H. *Analyst* **1998**, *123*, 2217.

(18) Klots, T. D.; Collier, W. B. *J. Mol. Struct.* **1996**, *380*, 1.

(19) Sommer, S.; Kamps, R.; Schumm, S.; Kleinermanns, K. F. *Anal. Chem.* **1997**, *69*, 1113.

(20) Spanget-Larsen, J.; Liang, D.; Chen, E.; Thulstrup, E. W. *Asian Chem. Lett.* **2000**, *4*, 121.

(21) Gastilovich, E. A.; Nurmukhametov, R. N.; Korol'kova, N. V.; Klimenko, V. G.; Serov, S. A. *Opt. Spectrosc.* **2003**, *95*, 353.

(22) Yamawaki, M.; Tatamitani, Y.; Doi, A.; Kasahara, S.; Baba, M. *J. Mol. Spectrosc.* **2006**, *238*, 49.

(23) Baba, M.; Mori, K.; Yamawaki, M.; Akita, K.; Ito, M.; Kasahara, S.; Yamanaka, T. *J. Phys. Chem. A* **2006**, *110*, 10000.

(24) Roos, B. O. Multiconfigurational (MC) Self-Consistent Field (SCF) Theory. In *European Summerschool in Quantum Chemistry*; Roos, B. O., Widmark, P.-O., Eds.; Lund University: Lund, 2003; Book II, pp 285−360.

(25) Andersson, K.; Malmqvist, P.-Å.; Roos, B. O. *J. Chem. Phys.* **1992**, *96*, 1218.

(26) (a) Runge, E.; Gross, E. K. U. *Phys. Rev. Lett.* **1984**, *52*, 997. (b) Marques, M. A. L.; Gross, E. K. U. *Annu. Rev. Phys. Chem.* **2004**, *55*, 427.

(27) Ljubić, I.; Sabljić, A. *J. Phys. Chem. A* **2005**, *109*, 8209.

(28) Ljubić, I.; Sabljić, A. *J. Phys. Chem. A* **2006**, *110*, 4524.

(29) Roos, B. O.; Andersson, K.; Fülscher, M. P.; Serrano-Andrés, L.; Pierloot, K.; Merchán, M.; Molina, V. *J. Mol. Struct. (THEOCHEM)* **1996**, *388*, 257.

(30) (a) Becke, A. D. *J. Chem. Phys.* **1993**, *98*, 5648. (b) Vosko, S. H.; Wilk, L.; Nusair, M. *Can. J. Phys.* **1980**, *58*, 1200. (c) Perdew, J. P. *Phys. Rev. B* **1986**, *33*, 8822.

(31) Wiberg, K. B.; Stratmann, R. E.; Frisch, M. J. *Chem. Phys. Lett.* **1998**, *297*, 60.

(32) Finley, J.; Malmqvist, P.-Å.; Roos, B. O.; Serrano-Andrés, L. *Chem. Phys. Lett.* **1998**, *288*, 299.

(33) Eberson, L.; Hartshorn, M. P.; Radner, F.; Merchán, M.; Roos, B. O. *Acta Chem. Scand.* **1993**, *47*, 176.

(34) Eberson, L.; González-Luque, R.; Merchán, M.; Radner, F.; Roos, B. O.; Shaik, S. *J. Chem. Soc., Perkin Trans. 2* **1997**, 463.

(35) Schaftenaar, G.; Noordik, J. H. *J. Comput.-Aided Mol. Des.* **2000**, *14*, 123.

(36) Roos, B. O. In *Advances in Chemical Physics: Ab Initio Methods in Quantum Chemistry II*; Lawley, K. P., Ed.; Wiley: New York, 1987; pp 399.

(37) Dunning, T. H. *J. Chem. Phys.* **1989**, *90*, 1007.

(38) Taylor, P. R. Accurate Calculations and Calibration. In *European Summerschool in Quantum Chemistry*; Roos, B. O., Widmark, P.-O., Eds.; Lund University: Lund, 2003; Book III, pp 665−674.

(39) Hariharan, P. C.; Pople, J. A. *Theor. Chem. Acc.* **1973**, *28*, 213.

(40) Forsberg, N.; Malmqvist, P.-Å. *Chem. Phys. Lett.* **1997**, *274*, 196.

(41) Ghigo, G.; Roos, B. O.; Malmqvist, P.-Å. *Chem. Phys. Lett.* **2004**, *396*, 142.

(42) Karlström, G.; Lindh, R.; Malmqvist, P.-Å.; Roos, B. O.; Ryde, U.; Veryazov, V.; Widmark, P.-O.; Cossi, M.; Schimmelpfennig, B.; Neogrady, P.; Seijo, L. *Comput. Mater. Sci.* **2003**, *28*, 222.

(43) Frisch, M. J.; Trucks, G. W.; Schlegel, H. B.; Scuseria, G. E.; Robb, M. A.; Cheeseman, J. R.; Montgomery, J. A., Jr.; Vreven, T.; Kudin, K. N.; Burant, J. C.; Millam, J. M.; Iyengar, S. S.; Tomasi, J.; Barone, V.; Mennucci, B.; Cossi, M.; Scalmani, G.; Rega, N.; Petersson, G. A.; Nakatsuji, H.; Hada, M.; Ehara, M.; Toyota, K.; Fukuda, R.; Hasegawa, J.; Ishida, M.; Nakajima, T.; Honda, Y.; Kitao, O.; Nakai, H.; Klene, M.; Li, X.; Knox, J. E.; Hratchian, H. P.; Cross, J. B.; Bakken, V.; Adamo, C.; Jaramillo, J.; Gomperts, R.; Stratmann, R. E.; Yazyev, O.; Austin, A. J.;

Cammi, R.; Pomelli, C.; Ochterski, J. W.; Ayala, P. Y.; Morokuma, K.; Voth, G. A.; Salvador, P.; Dannenberg, J. J.; Zakrzewski, V. G.; Dapprich, S.; Daniels, A. D.; Strain, M. C.; Farkas, O.; Malick, D. K.; Rabuck, A. D.; Raghavachari, K.; Foresman, J. B.; Ortiz, J. V.; Cui, Q.; Baboul, A. G.; Clifford, S.; Cioslowski, J.; Stefanov, B. B.; Liu, G.; Liashenko, A.; Piskorz, P.; Komaromi, I.; Martin, R. L.; Fox, D. J.; Keith, T.; Al-Laham, M. A.; Peng, C. Y.; Nanayakkara, A.; Challacombe, M.; Gill, P. M. W.; Johnson, B.; Chen, W.; Wong, M. W.; Gonzalez, C.; Pople, J. A. *Gaussian 03*, revision C.02; Gaussian, Inc.: Wallingford, CT, 2004.

(44) Malmqvist, P.-Å.; Roos, B. O. *Chem. Phys. Lett.* **1989**, *155*, 189.

(45) (a) Reppart, W. J.; Gallucci, J. C.; Lundstedt, A. P.; Gerkin, R. E. *Acta Crystallogr.* **1984**, *C40*, 1572. (b) Banerjee, A. *Acta Crystallogr.* **1973**, *B29*, 2070.

(46) Hubbard, C. R.; Mighell, A. D.; Pomerantz, I. H. *Acta Crystallogr*. **1978**, *B34*, 2381.

(47) Data taken from the Computational Chemistry Comparison and Benchmark DataBase (http://srdata.nist.gov/cccbdb/), a public service provided by the National Institute of Standards and Technology (NIST).

(48) Gerkin, R. E.; Lundstedt, A. P.; Reppart, W. J. *Acta Crystallogr*. **1984**, *C40*, 1892.

(49) Gerkin, R. E.; Reppart, W. J. *Acta Crystallogr*. **1986**, *C42*, 480.

(50) Ljubić, I.; Sabljić, A. *Chem. Phys.* **2005**, *309*, 157 and references therein.

(51) Scott, A. P.; Radom, L. *J. Phys. Chem.* **1996**, *100*, 16502.

(52) Ryzhikov, M. B.; Rodionov, A. N.; Rodin, O. G.; Shigorin, D. N. *Zh. Fiz. Khim.* **1989**, *63*, 534.

(53) Casida, M. E.; Jamorski, C.; Casida, K. C.; Salahub, D. R. *J. Chem. Phys.* **1998**, *108*, 4439.